JOURNAL OF MATERIALS SCIENCE 30 (1995) 6023–6027

Mechanical properties of β-Si_3N_4 whisker reinforced α′-SiAlON ceramics

SHYH-LUNG HWANG*, HUA-TAY LIN, P. F. BECHER
Metals and Ceramics Division, Oak Ridge National Laboratory, Oak Ridge, TN 37831-6068, USA

The effects of β-Si_3N_4 whisker additions on the mechanical properties of α′-SiAlON ceramics were studied. The room temperature fracture toughness and fracture strength of the composites increased with increasing whisker content, and were 6.5 MPa $m^{1/2}$ and 900 MPa, respectively, for the addition of 30 vol% whiskers. Although creep resistance of the composites was not enhanced at 1200 °C, the whisker additions were observed to be beneficial in reducing the oxidation induced slow crack growth of α′-SiAlON that occurred at 1300 °C, and thereby, improved the creep resistance of the composites at 1300 °C.

1. Introduction

α′-SiAlONs are α-Si_3N_4 solid solutions with the substitutions of Si by Al and N by O. The valence compensation is effected by incorporating the modifying cations such as Y or Ca into the interstices of the (Si, Al)–(N, O) network [1]. The discovery of α′-SiAlON, together with the β′-SiAlON, provided the possibility of obtaining dense silicon nitride ceramics with limited residue glassy phases using the transient liquid sintering method [2]. With excellent hardness at both room and elevated temperatures [3, 4] single phase α′-SiAlON ceramics have the potential to compete with other silicon nitride ceramics for high temperature structural applications, if their inherent brittleness can be improved.

In recent years, many studies have investigated the effects of whisker reinforcement in Si_3N_4 or β′-SiAlON ceramics [5–9]. It was found that improvements in mechanical properties, mainly in fracture toughness, could be achieved by incorporating either SiC or Si_3N_4 whiskers. The toughening mechanisms associated with whisker additions were found to be crack deflection, crack branching, crack bridging, as well as whisker pull-out, and were dependent upon the shape, size, as well as the volume fraction of whiskers [5–9].

This study was aimed at improving the fracture toughness of α′-SiAlON by the addition of β-Si_3N_4 whiskers. The room temperature mechanical properties and the high temperature flexural creep behaviour were studied. These results were then compared with the properties of other α′-SiAlON ceramics containing *in-situ* growth equiaxed β-Si_3N_4 grains.

2. Experimental procedures

2.1. Compositions

The compositions of materials studied herein lie on the Si_3N_4–Al_2O_3: AlN–YN: 3AlN plane (α′-plane) and are schematically represented in Fig. 1. Two sets of materials along the β–α′($m = 1.0$, $n = 1.7$) tie-line were prepared. The first set was prepared without the addition of β-Si_3N_4 whiskers and contains the β + α′ phase assemblages. The second set includes materials with the substitution of β phase in the first set by the β-Si_3N_4 whiskers. Since the compositions on the α′-plane can be represented by the formula $Y_{m/3}Si_{12-(m+n)}Al_{(m+n)}O_nN_{16-n}$, we use ($m$, n) to designate our materials. For example, 0717 represents the material with $m = 0.7$ and $n = 1.7$, and having an equilibrium phase assemblage of 70% α′-SiAlON and 30% β-Si_3N_4 according to Fig. 1. For materials with β-whisker substitution for *in-situ* growth of β-Si_3N_4, the material designations were prefixed by a letter "W".

Our selections of compositions with n values greater than 1.2 are based on the ability to densify the materials; in hot-pressing experiments, we observed that powder compacts with n values less than 1.2 usually could not be fully densified, no matter what hot-pressing schedules were used. Note that the ability to reach full density usually depends on the oxygen content of a powder compact, which is equal to $2n/(48 - n)$ for powder batches with proper excess oxygen compensation as described below.

With the presence of surface oxides on the starting Si_3N_4 powders, Si_3N_4 whiskers, and AlN powders, the resultant compositions are always out of the α′-plane and shift toward the SiO_2–Al_2O_3 line, if the initial powder batches are prepared based on the actual nitride contents in Si_3N_4 and AlN. To assure the formation of SiAlON ceramics with proper phase assemblages and with minimum grain boundary glassy phases, the overall compositions of the powder batches need to be brought back to the α′-plane by adding extra AlN. Note that the AlN–Al_2O_3 and AlN–SiO_2 lines intersect the α′-plane at their

* ORNL Postdoctoral Fellow, Oak Ridge Institute of Science and Technology, Oak Ridge Associated University.

0022–2461

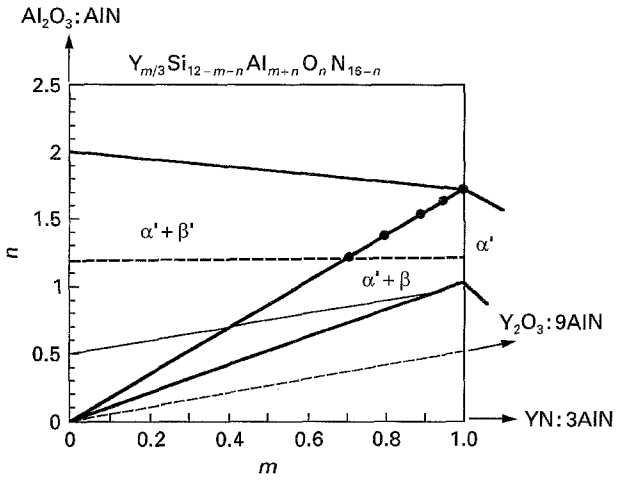

Figure 1 Phase diagram showing the compositions studied.

intermediate points, i.e. β60 and AlN:Al_2O_3. Due to the introduction of β60/Al_2O_3:AlN from this oxide compensation scheme, the final compositions will then be shifted away from the Si_3N_4 corner. To obtain a target composition, an adjustment of the initial composition then needs to be made in order to cope with this composition shift. For instance, to obtain composition 1017, we have to start with a composition with $m = 1.05$ and $n = 1.37$.

2.2. Materials processing

The compositions were prepared in 40 g batches from the starting powders. The oxygen contents (in wt %) were 1.43% (Si_3N_4), 0.54% (Si_3N_4 whisker) and 1.0% (AlN). The iron and calcium impurities were < 100 p.p.m. and < 50 p.p.m., respectively, in Si_3N_4 powders, and were < 700 p.p.m. and < 150 p.p.m., respectively, in Si_3N_4 whiskers. The purity of Al_2O_3 was 99.995% and that of Y_2O_3 was 99.9%. The average diameter of β-Si_3N_4 whiskers was ≈ 1.1 μm. The powders were attrition-milled in 2-propanol in a Teflon-lined steel jar of 0.7 l size using 700 g of silicon nitride milling balls (2 mm in diameter) for 2 h. After milling, the slurry was stirred in a Teflon beaker and dried on a hot plate. Dense specimens were obtained by hot-pressing 15 g charges using a high purity graphite die at 1700 °C for 1 h in 1.013×10^5 Pa of nitrogen. A hot-pressing load of ≈ 30 MPa was applied at 1400 °C and was released at 1000 °C during cooling. The heating rate during hot-pressing was $\approx 20\,°C\,min^{-1}$.

2.3. Characterizations

Flexure bars ($2.5 \times 3.3 \times 25$ mm) were machined from hot-pressed billets using diamond abrasive slicing and grinding wheels. The tensile surface was perpendicular to the hot-pressing direction. The tensile surfaces of the flexure bars were prepared by surface grinding in a direction parallel to the length of the bars with a 220 grit diamond resinoid bonded wheel. The room temperature flexural strength was evaluated at a cross-head speed of 1.67×10^{-3} mm s^{-1} using a four-point bending fixture with inner and outer span of 6.35 mm and 19.05 mm, respectively. Hardness and indentation fracture toughness was measured on the polished sections perpendicular to the hot-pressing direction by Vickers indenter with 20 kg load. Toughness values were calculated according to Reference 10, assuming a Young's modulus of 350 GPa [11].

Flexural creep tests were conducted at temperatures of 1200 and 1300 °C and at stresses from 75 to 250 MPa in air. The bend bars were loaded in a fully dense sintered α-SiC four-point bending fixture with sintered α-SiC loading pins at inner and outer spans of 19 and 38 mm respectively. The desired stresses were applied to the test specimens through a sintered α-SiC push rod via a dead weight loading system. The outer fibre displacement of the bend bars was measured by a high-temperature three-probe extensometer whose output was continuously recorded. The outer fibre stress and corresponding deformation strain were calculated based upon the procedures described by Hollenberg *et al.* [12]. The microstructures of the as-sintered and crept specimens, as well as the indentation cracks were examined using scanning electron microscopy (SEM).

3. Results and discussions

3.1. Microstructures

All materials studied here reached full density in hot-pressing, as evident from the lack of any microporosity on polished sections analysed by SEM. X-ray diffraction analyses showed no remaining α-Si_3N_4. All specimens had final phase assemblages consisting of α′-SiAlON, β-Si_3N_4 (or β-Si_3N_4 whiskers), and traces of 12H polytypoid of AlN. Since all powder batches in our experiments were carefully compensated for the excess oxygen, the presence of 12H phase implies the presence of oxygen-rich residue grain boundary glassy phases in the as-hot pressed specimens.

A SEM micrograph of material W0717, showing the typical microstructure of β-Si_3N_4 whisker reinforced α′-SiAlON ceramics hot-pressed at 1700 °C, is shown in Fig. 2(a). As shown, the dark β-Si_3N_4 whiskers are uniformly distributed within the grey α′-matrix without any whisker agglomerates. SEM observations at high magnifications (> 20 K) revealed that there were only very small amounts of triple point phases and the amount of residue glassy phase content was very limited, estimated to be less than 1 vol %. Apparently the compositional compensation to control excess oxygen in our experiments was sufficient to result in such a low residue glassy phase content. Theoretically, if the excess oxygen is well compensated for, all liquid phases formed in the sintering cycle should be completely incorporated into the α′-SiAlON structure. However, kinetically, this is difficult [13, 14]. The β-Si_3N_4 whiskers were oriented with the long axis predominantly perpendicular to the hot-pressing direction, as shown in the fracture surface in Fig. 2(b). In contrast to the smooth surface of the starting β-whiskers, the whisker surface in the composite materials appeared to be rather rugged (Fig. 2(c)), with many impress marks formed in the hot-pressing cycle probably by a pressure–solution process [15]. The

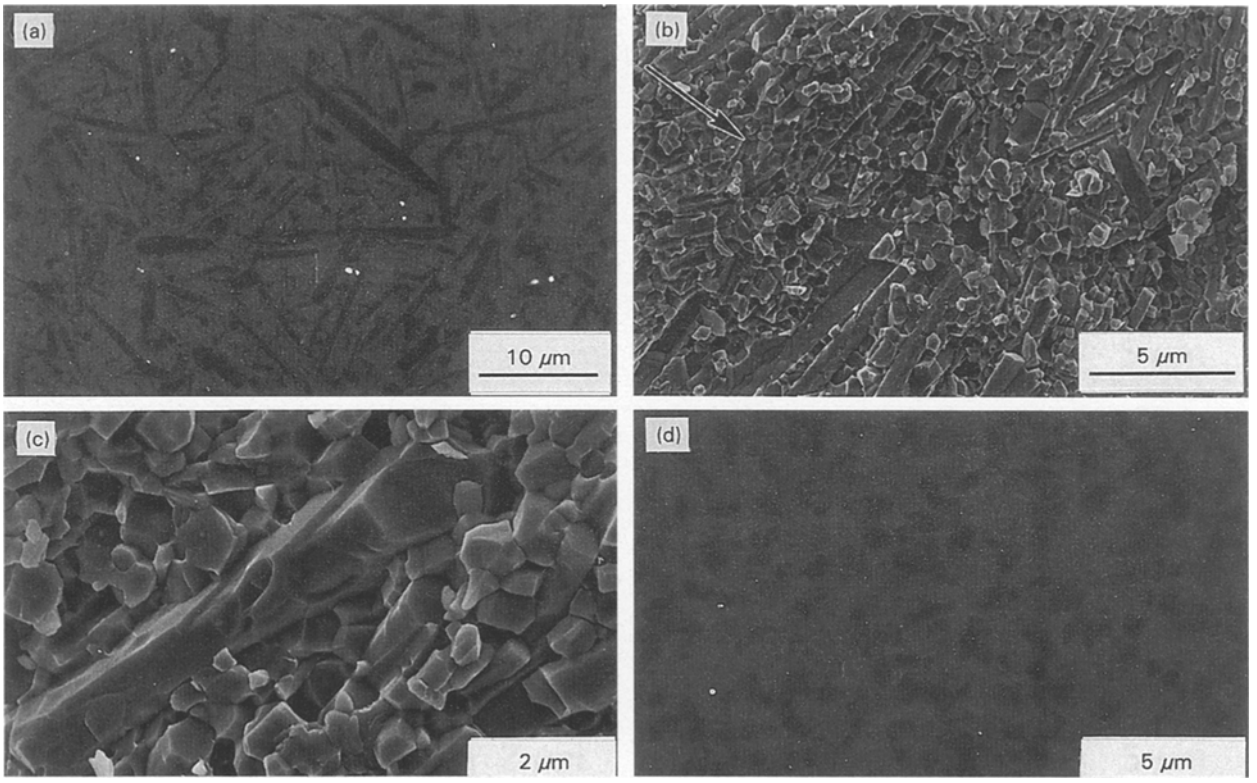

Figure 2 SEM micrographs showing (a) uniform whisker distribution, (b) whisker alignment on the hot-pressing plane, and (c) surface roughness of β-Si_3N_4 whiskers in material W0717, as well as (d) rounded morphology of the in-site growth β-Si_3N_4 grains in material 0717. The hot-pressing direction is marked with an arrow.

α′-grains were equiaxed and had an average size of ~0.6 μm, which remained virtually invariant with increasing whisker content.

In comparison with the fibrous morphology of whiskers, the *in-situ* precipitated β-Si_3N_4 grains were typically small (~0.6 μm) and equiaxed, as shown in the polished section of material 0717 in Fig. 2(d). This type of β morphology indicated the difficulties in developing elongated β-Si_3N_4 grains without the presence of excess glassy phases in our materials. In the literature, the elongated β-Si_3N_4/β′-SiAlON grains only arose in materials fabricated either without oxygen compensation or with excess amount of oxide sintering additives [3, 4].

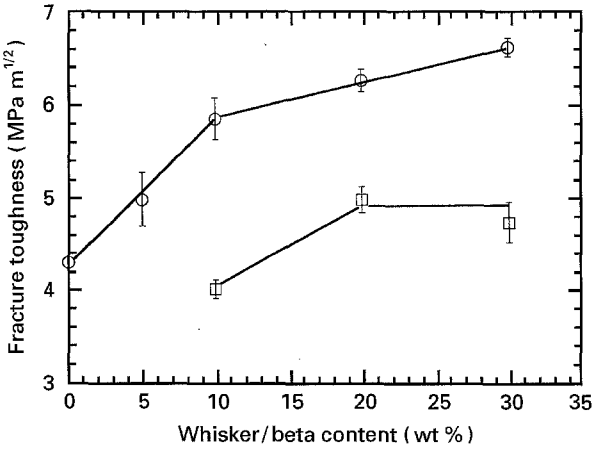

Figure 3 Room temperature fracture toughness of α′-SiAlON reinforced with (○) β-Si_3N_4 whiskers or (□) *in-situ* growth of β-Si_3N_4.

3.2. Room temperature mechanical properties

All materials studied here had a Vickers hardness (H_{V20}) of ~20.5 GPa. This hardness value was basically independent of the amount (up to 30%) of either β-Si_3N_4 whiskers or *in-situ* precipitated β-Si_3N_4 grains in the α′-matrix. Similar Vickers hardness was reported in hot isostatically pressed α′-SiAlON with trace amounts of glassy grain boundary phases [16].

The indentation fracture toughness of β-Si_3N_4 whisker-reinforced α′-SiAlON ceramics are shown in Fig. 3. The fracture toughness of the unreinforced α′-SiAlON was ~4.3 MPa m$^{1/2}$. The toughness of the whisker-reinforced composites relative to the α′-SiAlON increased rapidly for 5 and 10% additions of whiskers, and then more slowly to 30% whiskers. The toughness value at 30% whiskers was ~6.5 MPa m$^{1/2}$, representing a toughness improvement of ~50% compared to the α′-matrix. Compared to other α′-SiAlON ceramics with or without large amounts of grain boundary glassy phases, this toughness value represents a substantial improvement [3, 4, 16, 17].

Contrary to the case with whisker additions, the toughening effect from the *in-situ* precipitated equiaxed β-Si_3N_4 grains seemed to be limited. The maximum toughness occurred at 20% β-Si_3N_4 and

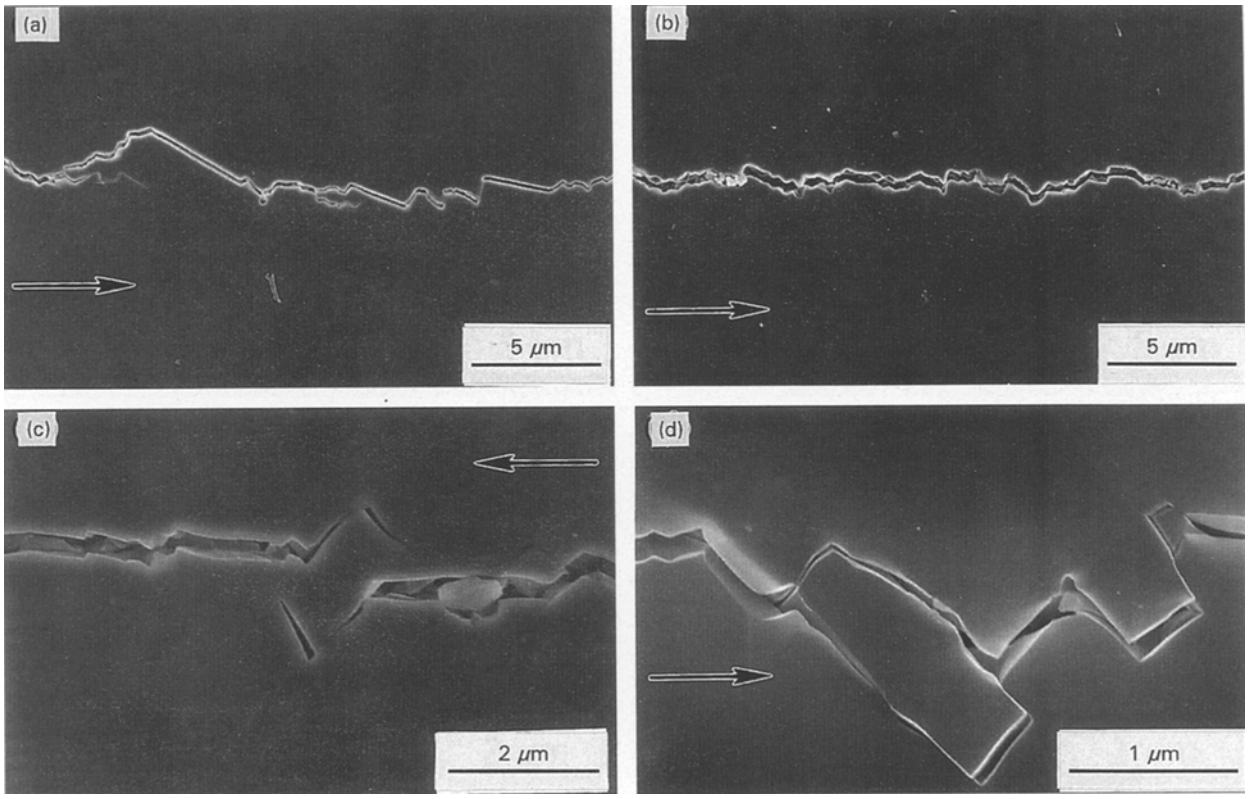

Figure 4 SEM micrographs showing the indentation-induced crack trajectories in materials (a) W0717 and (b) 0717, as well as (c) crack bridging and (d) whisker pullout occurred in material W0717. The propagating direction of each crack is marked with an arrow.

was $\sim 5\ MPa\,m^{1/2}$. The different toughening behaviour between this set of materials and that with β-Si_3N_4 whisker additions indicates the importance of the morphology of the reinforcing phase in toughening; the larger diameter and higher aspect ratio of β-Si_3N_4 whiskers would cause more crack deflection and branching, thereby consuming more fracture energy. This was evident from comparing the crack trajectories of materials W0717 and 0717 shown in Fig. 4(a and b); the crack paths in W0717 were much more tortuous than those in 0717. Besides crack deflection and branching, other more efficient toughening mechanisms such as crack bridging by whiskers as well as whisker pull-out were also operative, as shown in Fig. 4(c and d) [18]. However, the occurrences of these two toughening processes may be limited by the rough whisker surfaces.

In a manner similar to the fracture toughness, the room temperature flexure strength of β-Si_3N_4 whisker reinforced α'-SiAlON ceramics increased with whisker content. As shown in Fig. 5, the composite strength increased from ~ 600 MPa for the α' matrix to ~ 900 MPa with 30% whisker addition. This extent of strength improvement, $\sim 50\%$, was similar to that observed in the indentation fracture toughness. This result also reflected the merits of the powder processing in the present experiments, which resulted in a homogeneous distribution of whiskers in the composites. The strength degradation found in the β-Si_3N_4 or SiC whisker reinforced β-Si_3N_4 ceramics was attributable to the formation of large processing flaws usually associated with whisker agglomerates retained from the starting materials [6–10].

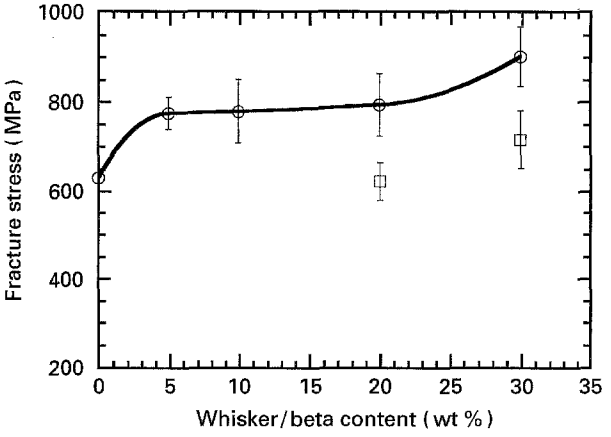

Figure 5 Room temperature fracture strength of α'-SiAlONs reinforced with (○) β-Si_3N_4 whiskers or (□) *in-situ* growth of β-Si_3N_4.

3.3. High temperature creep behaviour

Fig. 6 shows the creep results, at 1200 °C and 1300 °C in air, for both the α'-SiAlON matrix and the α'-SiAlON composites reinforced with 10 and 30 vol % β-Si_3N_4 whiskers. As shown, the creep resistance of α'-SiAlON was not altered by the incorporation of β-Si_3N_4 whiskers at 1200 °C, suggesting that the higher Fe/Ca impurity levels in the starting β-Si_3N_4 whiskers might lower the viscosity of the intergranular glassy phases and thus offset the pinning effect of whiskers as seen in the SiC reinforced Al_2O_3 composites [19]. The stress exponent was ~ 1 at 1200 °C, indicating that the creep controlling mechanism in these materials was diffusional, or viscous creep processes. This was evident by the SEM micrograph

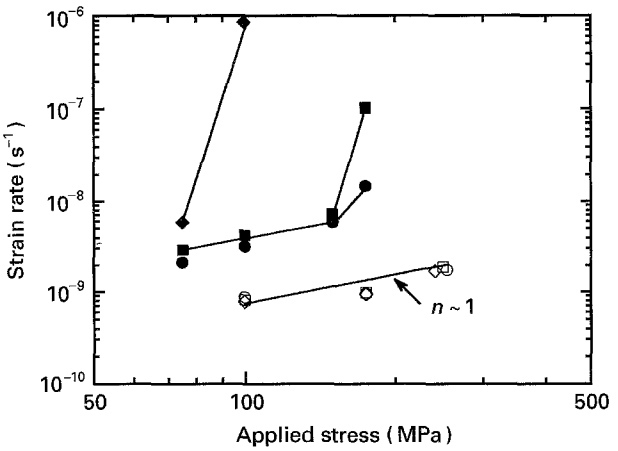

Figure 6 Strain rate versus stress curves of α′-SiAlONs reinforced with β-Si_3N_4 whiskers at 1200 and 1300 °C. ◇ 0 vol %, 1200 °C; ◆ 0 vol %, 1300 °C; □ 10 vol %, 1200 °C; ■ 10 vol %, 1300 °C; ○ 30 vol %, 1200 °C; ● 30 vol %, 1300 °C.

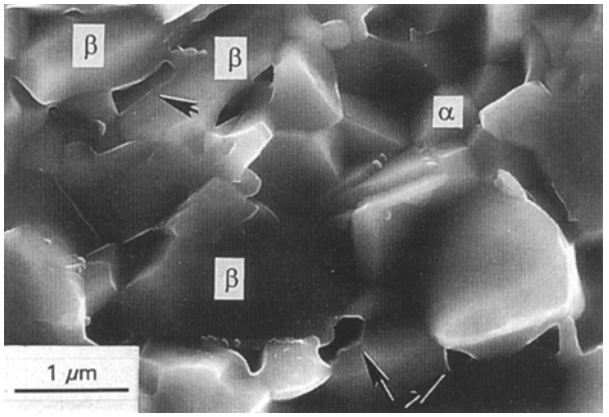

Figure 7 SEM micrograph showing the crack-like cavities at grain boundary or whisker/matrix interface.

of the α′-SiAlON matrix or composites showing crack like cavities at the grain boundaries or at the whisker/matrix interfaces (Fig. 7).

On the other hand: the creep rate of the α′-SiAlON matrix at 1300 °C was much higher than that with the β-Si_3N_4 whisker additions. The creep rupture life of α′-SiAlON matrix at 1300 °C at stresses $\geqslant$ 100 MPa was $<$ 1 h and was mainly due to the occurrence of oxidation-induced damages which were evident from the SEM observations of the crept materials. The creep rate of α′-SiAlON composites was much lower than the α′-SiAlON matrix and was basically independent of the whisker content. The stress exponent was $\sim$ 1 at stresses $\leqslant$ 150 MPa and was $>$ 3 at stresses $>$ 150 MPa. The high stress exponent was accompanied by higher creep rates. The higher stress exponent plus higher creep rate were usually attributed to the enhanced creep cavitation and crack growth as seen in the SiC whisker reinforced Si_3N_4 or Al_2O_3 composites [19, 20].

The α′-SiAlON ceramics were known to exhibit poor oxidation resistance at temperatures $\geqslant$ 1300 °C [21]. As a result, the oxidation-induced damage zone formed at 1300 °C causes the catastrophic failure of α′-SiAlON matrix by the slow crack growth (SCG) process. On the other hand, the β-Si_3N_4 whisker reinforcement, resulting in an increase in fracture resistance (Fig. 3), reduced the susceptibility of α′-SiAlON matrix to oxidation-induced SCG process and thus improves the creep performance at 1300 °C.

4. Summary

Externally added β-Si_3N_4 whiskers were found to be more effective than the *in-situ* growth of β-Si_3N_4 grains in toughening α′-SiAlON. The room temperature fracture toughness and fracture strength of the composites increased with increasing whisker content, and were 6.5 MPa $m^{1/2}$ and 900 MPa, respectively, for the addition of 30% β-Si_3N_4 whiskers. Although creep resistance of the composites was not enhanced by whisker addition, the susceptibility to the oxidation induced slow crack growth process of the α′-SiAlON matrix seemed to be reduced by whisker additions.

Acknowledgements

The authors thank Drs H. Cai and K. Plucknett for reviewing the manuscript. Shyh-Lung Hwang was supported in part by an appointment to the Oak Ridge National Laboratory Postdoctoral Research Program administrated jointly by Oak Ridge Institute of Science and Technology and Oak Ridge National Laboratory. This research was supported by the US Department of Energy, Office of Basic Energy Sciences, Division of Materials Sciences, and Office of Transportation Technologies, as part of the Ceramic Technology Project of the Propulsion System Materials Program, under Contract DE-AC05-84OR21400 with Lockhead Martin Energy Systems, Inc.

References

1. S. HAMPSHIRE, H. K. PARK, D. P. THOMPSON and K. H. JACK, *Nature*, **274** (1978) 880.
2. K. H. JACK, *J. Mater. Sci.* **11** (1976) 1135.
3. T. EKSTROM and J. PERSSON, *J. Amer. Ceram. Soc.* **73** (1990) 2834.
4. T. EKSTROM and M. NYGREN, *ibid.* **75** (1992) 259.
5. P. D. SHALEK, J. J. PETROVIC, G. F. HURLEY and F. D. GAC, *Amer. Ceram. Soc. Bull.* **65** (1986) 351.
6. S. T. BULJAN, J. G. BALDONI and M. L. HUCKABEE, *ibid.* **66** (1987) 347.
7. P. SAJGALIK and J. DUSZA, *J. Mater. Sci.* **10** (1991) 776.
8. P. SAJGALIK and J. DUSZA, *J. Eur. Ceram. Soc.* **5** (1989) 321.
9. D. MUSCAT, M. D. PUGH and R. A. L. DREW, in "Ceramic transactions, Vol. 19, Advanced composite materials", edited by M. D. Sacks (American Ceramic Society, Westerville, OH, 1991) p. 137.
10. A. G. EVANS and E. A. CHARLES, *J. Amer. Ceram. Soc.* **59** (1976) 371.
11. O. YEHESKEL and Y. GEFEN, *Mater. Sci. Eng.* **71** (1985) 95.
12. G. W. HOLLENBERG, G. R. TERWILLIGER and R. S. GORDON, *J. Amer. Ceram. Soc.* **54** (1971) 196.
13. R. RAJ, *ibid.* **64** (1981) 245.
14. R. RAJ and F. F. LANGE, *Acta Metall.* **201** (1981) 1993.
15. M. S. PATERSON, *Review of Geophysics and Space Physics* **11** (1973) 355.
16. A. BARTEK, T. EKSTROM, H. HERBERTSSON and T. JOHANSSON, *J. Amer. Ceram. Soc.* **75** (1992) 432.
17. T. EKSTROM and P-O. OLSSON, *ibid.* **72** (1989) 1722.
18. P. F. BECHER, E. R. FULLER and P. ANGELINI, *ibid.* **74** (1991) 2131.
19. H. T. LIN and P. F. BECHER, *ibid.* **74** (1991) 1886.
20. B. H. HOCKEY, S. M. WIEDERHORN, W. LIU, J. G. BALDONI and S. T. BULJAN, *J. Mater. Sci.* **26** (1991) 3931.
21. M. H. LEWIS and P. BARNARD, *ibid.* **15** (1980) 443.

Received 22 December 1994
and accepted 2 May 1995